

High-Pressure Hydrogen Sulfide by Diffusion Quantum Monte Carlo

Sam Azadi*

*Department of Materials Science, Royal School of Mines,
Thomas Young Center, London Centre for Nanotechnology,
Imperial College London, London SW7 2AZ, United Kingdom*

Thomas D. Kühne

*Dynamics of Condensed Matter, Department of Chemistry,
University of Paderborn, Warburger Str. 100, D-33098 Paderborn, Germany and
Paderborn Center for Parallel Computing and Institute for Lightweight Design with Hybrid Systems,
University of Paderborn, Warburger Str. 100, D-33098 Paderborn, Germany*

(Dated: October 13, 2021)

We use the diffusion quantum Monte Carlo to revisit the enthalpy-pressure phase diagram of the various products from the different proposed decompositions of H₂S at pressures above 150 GPa. Our results entails a revision of the ground-state enthalpy-pressure phase diagram. Specifically, we find that the C2/c HS₂ structure is persistent up to 440 GPa before undergoing a phase transition into the C2/m phase. Contrary to density functional theory, our calculations suggest that the C2/m phase of HS is more stable than the I4₁/amd HS structure over the whole pressure range from 150 to 400 GPa. Moreover, we predict that the Im-3m phase is the most likely candidate for H₃S, which is consistent with recent experimental x-ray diffraction measurements.

I. INTRODUCTION

Back in 1968, Ashcroft predicted that according to the BCS theory¹, dense hydrogen would not only be metallic², but more importantly also a high-temperature superconductor³. Since recently it has been shown that dissociation is a necessary condition for the metallization of hydrogen^{4,5}, the necessary pressure to cause bandgap closure has remained impractical high, so that metallic hydrogen has only been realized at finite-temperature⁶⁻¹⁰. Yet, an appealing way to circumvent the high pressures required to metallize hydrogen is to precompress it in hydrogen-rich systems^{11,12}, since, in general, the electronic density of states is high and the electron-phonon interactions are strong¹³.

In fact, pressurized Hydrogen-rich materials have demonstrated to be rather promising candidates for high- T_c superconductivity^{12,16-22}. In particular, Drozdov and Eremets reported that at pressures around 200 GPa, dense hydrogen sulphide becomes metallic and superconducting with a critical temperature (T_c) of 203 K²³, which is well above the highest T_c of 133 K and 164 K that were achieved in cuprates²⁴ at ambient²⁵ and high pressures²⁶ respectively. Recent experimental results indicate that the superconducting state of H₃S adopts a body-centered cubic (BCC) structure²⁷.

However, nearly all of the recent calculations on Hydrogen-rich systems are based on the single-particle mean-field theories such as density-functional theory (DFT)^{21,22,28-35}. Even though formally exact, the exact exchange and correlation (XC) functional is unknown from the outset and needs to be approximated, which affects both the relative stabilities of the different crystal structures. Indeed, for dense hydrogen-rich materials a significant dependence on the particular of XC functional was established^{4,36-39}.

Therefore, in this paper we revisit the stability of the individual products originating from the various proposed decompositions of H₂S for pressures above 150 GPa by means of highly accurate diffusion Monte Carlo (DMC) simulations. Using the DMC method^{40,41}, the electronic many-body Schrödinger equation is solved stochastically, which have yielded very accurate total energies for atoms^{42,43}, molecules⁴⁴⁻⁴⁶, crystals^{39,47-49} including hydrogen-rich materials at very high pressure^{5,50-52}.

II. COMPUTATIONAL DETAILS

At first, all of the examined structures were determined by relaxing the internal parameters of each phase within DFT at fixed external pressure. The DFT calculations were all conducted within the pseudopotential and plane-wave approach using the CASTEP code⁵³. Specifically, ultrasoft pseudopotentials were employed together with an energy cutoff of 1000 eV⁵⁴. The exact XC functional was substituted by the generalized gradient approximation of Perdew-Burke-Ernzerhof (PBE).⁵⁵ The geometry and cell optimizations were conducted using a dense $16 \times 16 \times 16$ \mathbf{k} -point mesh to sample the Brillouin zone, while the nuclear forces and components of the stress tensor were converged to 0.01 eV/Å and 0.01 GPa, respectively.

The CASINO code was used to perform fixed-node DMC simulations with a trial wave function of the Slater-Jastrow (SJ) form⁵⁶,

$$\Psi_{\text{SJ}}(\mathbf{R}) = \exp[J(\mathbf{R})] \det[\psi_n(\mathbf{r}_i^\uparrow)] \det[\psi_n(\mathbf{r}_j^\downarrow)], \quad (1)$$

where \mathbf{R} is a $3N$ -dimensional vector containing the positions of all N electrons, \mathbf{r}_i^\uparrow the position of the

i 'th spin-up electron, \mathbf{r}_j^\downarrow the position of the j 'th spin-down electron, $\exp[J(\mathbf{R})]$ a Jastrow factor, while $\det[\psi_n(\mathbf{r}_i^\uparrow)]$ and $\det[\psi_n(\mathbf{r}_j^\downarrow)]$ are Slater determinants made of spin-up and spin-down one-electron wave functions. These orbitals were obtained from PBE-DFT calculations performed with the CASTEP plane-wave code⁵³, in conjunction with Trail-Needs Hartree-Fock pseudopotentials^{57,58}. For the purpose to approach the complete basis set limit⁵⁹, a large energy cut-off of 4000 eV have been chosen. The resulting plane-wave orbitals were subsequently transformed into a localized "blip" polynomial basis⁶⁰.

The Jastrow factor within Eq. 1 is a positive, symmetric, explicit function of interparticle distances. The employed Jastrow factor includes polynomial one-body electron-nucleus (1b), two-body electron-electron (2b) and three-body electron-electron-nucleus (3b) terms, as well as plane-wave expansions of the electron-electron separation known as p terms⁶¹. These p terms build long-ranged correlations into the Jastrow factor and thus significantly improve the wave function and variational energy. We also investigated the effect of the inhomogenous backflow (BF) coordinate transformation on the VMC and DMC total energies⁶². Our BF transformation includes electron-electron and electron-proton terms and is given by

$$\mathbf{X}_i(\{\mathbf{r}_j\}) = \mathbf{r}_i + \boldsymbol{\xi}_i^{(e-e)}(\{\mathbf{r}_j\}) + \boldsymbol{\xi}_i^{(e-P)}(\{\mathbf{r}_j\}), \quad (2)$$

where $\mathbf{X}_i(\{\mathbf{r}_j\})$ is the transformed coordinate of electron i , which depends on the full configuration of the system $\{\mathbf{r}_j\}$. The vector functions $\boldsymbol{\xi}_i^{(e-e)}(\{\mathbf{r}_j\})$ and $\boldsymbol{\xi}_i^{(e-P)}(\{\mathbf{r}_j\})$ are the electron-electron and electron-proton backflow displacements of electron i . They are parameterized as

$$\boldsymbol{\xi}_i^{(e-e)}(\{\mathbf{r}_j\}) = \sum_{j \neq i}^{N_e} \alpha_{ij}(r_{ij}) \mathbf{r}_{ij} \quad (3)$$

and

$$\boldsymbol{\xi}_i^{(e-P)}(\{\mathbf{r}_j\}) = \sum_I^{N_P} \beta_{iI}(r_{iI}) \mathbf{r}_{iI}, \quad (4)$$

where $\alpha_{ij}(r_{ij})$ and $\beta_{iI}(r_{iI})$ are polynomial functions of electron-electron and electron-proton distances that contains variational parameters. All adjustable parameters in the Jastrow factor and backflow terms were optimized by minimizing the variance as well as the variational energy at the VMC level^{63,64}. If not explicitly stated otherwise, all of our calculations were conducted using the SJ trail wave function including 1b, 2b, 3b and p terms augmented by the BF coordinate transformation.

Beside the usage of twist-averaged boundary conditions (TABC) to correct finite-size errors⁶⁵, we extrapolated the energy per atom to the thermodynamic limit by fitting our twist-averaged DMC results for different system sizes to $E(N) = aN^{-b} + E(\infty)$, where a and b are fitting parameters and $E(\infty)$ is the eventual energy

per atom in the infinite-system limit. Depending on simulation cell size, we used 8, 12 and 16 randomly chosen twists⁶⁶. The enthalpy was evaluated by differentiating the polynomial fit of our the finite-size-corrected DMC energies as a function of volume.

III. RESULTS AND DISCUSSION

A. DMC Total Energies

P(GPa)	E(N_1)	E(N_2)	E(N_3)	E(∞)
150	-187.6003(8)	-187.3893(6)	-187.2745(6)	-187.169(2)
200	-186.9612(8)	-186.7573(8)	-186.6484(5)	-186.546(2)
250	-186.3569(9)	-186.1696(8)	-186.0580(6)	-185.964(2)
300	-185.7804(8)	-185.6074(6)	-185.4851(7)	-185.399(2)

TABLE I. Total energies of the C2/m phase of HS₂ at the DMC level of theory for four different pressures. The energies are given in eV/atom and are calculated for $N_1 = 48$, $N_2 = 96$ and $N_3 = 192$ particles in the unit cell, respectively. The extrapolated DMC energy at the infinite system size limit is denoted by $E(\infty)$.

In the following, we are revisiting the crystal structures of Ref. 29. Specifically, we begin with investigating the monoclinic C2/c and C2/m structures of HS₂. The resulting total energies as a function of pressure at the DMC level of theory for the two HS₂ structures at different system sizes and the extrapolation to the thermodynamic limit are shown in Table I and II, respectively.

P(GPa)	E(N_1)	E(N_2)	E(N_3)	E(∞)
150	-187.757(1)	-187.5549(8)	-187.4934(6)	-187.469(2)
200	-187.254(1)	-186.9123(8)	-186.8828(5)	-186.817(2)
250	-186.767(1)	-186.3066(7)	-186.2809(6)	-186.187(2)
300	-186.348(1)	-185.7316(7)	-185.6965(5)	-185.572(2)

TABLE II. The DMC total energies of the C2/c HS₂ structure at four distinct pressures. The energies are calculated for $N_1 = 24$, $N_2 = 96$ and $N_3 = 192$ particles in the unit cell, respectively. The extrapolated DMC energy at the infinite system size limit is denoted by $E(\infty)$. All energies are in eV/atom.

Comparing the DMC results for the C2/m and C2/c structures of HS₂, we find that at the same pressure, the total energy of the C2/c phase is throughout lower than that of the C2/m structure. Starting from 150 GPa, the difference is as large as 299.7 meV/atom, but is strictly decreasing to 173 meV/atom for 300 GPa.

The DMC total energies for the C2/m and I4₁/amd structures of HS are shown in Tables III and IV, respectively. As before, all energies are calculated for different number of particles in the unit cell and extrapolated to the thermodynamic limit. Even though the difference in varying, the C2/m structure of HS is energetically

P(GPa)	E(N_1)	E(N_2)	E(N_3)	E(∞)
150	-144.6139(8)	-144.5199(5)	-144.4455(4)	-144.398(1)
200	-143.9814(7)	-143.8912(6)	-143.8268(5)	-143.781(1)
250	-143.2503(8)	-143.1232(6)	-143.0780(5)	-143.014(1)
300	-142.8490(7)	-142.6977(6)	-142.6069(5)	-142.531(1)

TABLE III. Total energies of the C2/m phase of HS at the DMC level of theory for four different pressures. The energies are given in eV/atom and are calculated for $N_1 = 64$, $N_2 = 128$ and $N_3 = 256$ particles in the unit cell, respectively. The extrapolated DMC energy at the infinite system size limit is denoted by $E(\infty)$.

throughout lower by about 500 meV/atom than the corresponding I4₁/amd phase. More precisely, at a pressure of 150, 200, 250 and 300 GPa, the differences between the two structures are 580, 634, 479 and 582 meV/atom, respectively.

P(GPa)	E(N_1)	E(N_2)	E(N_3)	E(∞)
150	-145.251(1)	-144.5755(8)	-144.1563(5)	-143.819(2)
200	-144.988(1)	-144.1049(9)	-143.5889(5)	-143.147(2)
250	-144.671(1)	-143.6350(9)	-143.0537(6)	-142.535(2)
300	-144.332(1)	-143.1536(9)	-142.5379(5)	-141.948(2)

TABLE IV. The DMC total energies of the I4₁/amd HS structure at four distinct pressures. The energies are calculated for $N_1 = 32$, $N_2 = 64$ and $N_3 = 128$ particles in the unit cell, respectively. The extrapolated DMC energy at the infinite system size limit is denoted by $E(\infty)$. All energies are in eV/atom.

Among the various potential products of the decomposition of H₂S, H₃S is a particular intriguing candidate for conventional, but high-temperature BCS superconductivity due to its high-frequency phonon modes. Interestingly, recent theoretical crystal structure prediction simulations suggested that at high-pressure, H₃S in its trigonal R3m and cubic Im-3m structures are the most likely products of the decomposition of H₂S²⁸. Even though chemical somewhat counter-intuitive, we also revisiting here the proposed structures by means of DMC.

P(GPa)	E(N_1)	E(N_2)	E(N_3)	E(∞)
150	-80.0626(6)	-79.8131(5)	-79.7489(3)	-79.624(1)
200	-79.7696(6)	-79.5045(5)	-79.4268(3)	-79.294(1)
250	-79.4855(7)	-79.2093(4)	-79.1287(3)	-78.991(1)
300	-79.1996(7)	-78.9137(5)	-78.8325(3)	-78.689(1)

TABLE V. Total energies of the R3m phase of H₃S at the DMC level of theory for four different pressures. The energies are given in eV/atom and are calculated for $N_1 = 48$, $N_2 = 96$ and $N_3 = 192$ particles in the unit cell, respectively. The extrapolated DMC energy at the infinite system size limit is denoted by $E(\infty)$.

The corresponding total energies, as computed by DMC, are listed in Tables V and VI, respectively.

We find that in thermodynamic limit, the Im-3m struc-

P(GPa)	E(N_1)	E(N_2)	E(N_3)	E(∞)
150	-79.3944(5)	-79.6212(4)	-79.6717(3)	-79.785(1)
200	-79.0955(5)	-79.3326(4)	-79.3767(3)	-79.495(1)
250	-78.7941(5)	-79.0420(4)	-79.0851(3)	-79.209(1)
300	-78.4924(4)	-78.7555(4)	-78.7934(3)	-78.925(1)

TABLE VI. The DMC total energies of the Im-3m pH₃S structure at four distinct pressures. The energies are calculated for $N_1 = 64$, $N_2 = 128$ and $N_3 = 256$ particles in the unit cell, respectively. The extrapolated DMC energy at the infinite system size limit is denoted by $E(\infty)$. All energies are in eV/atom.

ture is energetically more favorable than the R3m phase of H₃S over the whole pressure range considered here, and that the difference slightly widens with increasing pressure.

B. Backflow Wavefunction

However, due to the necessary fixed-node approximation in order to cope with the infamous fermion sign-problem^{67,68}, the fixed-node DMC method samples the variationally optimal many-electron wave function, which is consistent with an *a priori* given nodal surface of a presumed trial wave function, instead of the exact ground-state wave function⁴⁰. [The nodal surface of an N -electron wave function $\Psi(\mathbf{r}_1, \mathbf{r}_2, \dots, \mathbf{r}_N)$ is the $(3N - 1)$ -dimensional hypersurface on which Ψ is zero.] Therefore, the accuracy of the presumed trial wave function, determines the quality the eventual results via the nodal surface, which represents the sole approximation of the employed fixed-node DMC method.

As already alluded to previously, using the so called BF coordinate transformation⁶⁹⁻⁷¹, the orbitals in the Slater determinant are evaluated not at the actual electron positions, but on quasi-electron positions that are functions of all the particle coordinates. However, the BF function, which describes the offset of the quasi-electron coordinates relative to the actual coordinates, contains free parameters, which are determined by a variational optimization of the trial wave function. In this way, the nodes of the BF trial wave function are no longer fixed, but do have some flexibility to move during the trial wave function optimization in order to further minimize the variational energy.

Here, we have employed a large variety of different trial wave functions within our VMC and DMC energies of HS₂ and H₃S, which are the systems with of lowest and highest hydrogen densities we have considered. Specifically, we applied SJ-type trial wave functions including one- and two-body terms (SJ(1b+2b)), an additional three-body term (SJ(1b+2b+3b)), as well as the respective versions that are augmented by a p -term denoted as SJ(1b+2b+ p) and SJ(1b+2b+3b+ p), respectively. In addition, Backflow-Slater-Jastrow (BSJ) trial wave functions including one- and two-body terms (BSJ(1b+2b))

WF	VMC	DMC	variance
SJ(1b+2b)	-81.9882(5)	-82.1819(5)	6.97(2)
SJ(1b+2b+p)	-82.0508(3)	-82.1848(5)	6.22(4)
SJ(1b+2b+3b)	-82.0150(4)	-82.1886(5)	6.54(3)
SJ(1b+2b+3b+p)	-82.0772(3)	-82.1932(4)	5.82(2)
BSJ(1b+2b)	-82.0806(3)	-82.2259(4)	5.10(3)
BSJ(1b+2b+3b+p)	-82.1683(3)	-82.2423(4)	4.17(4)

TABLE VII. The VMC and DMC total energies for the C2/m phase of HS₂ as calculated using the SJ(1b+2b), SJ(1b+2b+p), SJ(1b+2b+3b), SJ(1b+2b+3b+p), as well as BSJ(1b+2b) and BSJ(1b+2b+3b+p) trial wave functions. All energies are in Hartree per primitive unit cell.

and the subsequent variant including an additional three-body and the p term (BSJ(1b+2b+3b+p)) are considered. The resulting VMC and DMC total energies for the C2/m phase of HS₂ and Im-3m H₃S structure are listed in Tables VII and VIII, respectively. The energy

WF	VMC	DMC	variance
SJ(1b+2b)	-23.1044(3)	-23.1650(2)	4.21(4)
SJ(1b+2b+p)	-23.1223(2)	-23.1663(2)	3.75(1)
SJ(1b+2b+3b)	-23.1134(2)	-23.1674(3)	3.90(2)
SJ(1b+2b+3b+p)	-23.1307(2)	-23.1680(2)	3.54(1)
BSJ(1b+2b)	-23.1381(2)	-23.1803(3)	2.81(2)
BSJ(1b+2b+3b+p)	-23.1645(2)	-23.1856(1)	2.278(9)

TABLE VIII. The VMC and DMC total energies of the Im-3m H₃S structure as calculated using the SJ(1b+2b), SJ(1b+2b+p), SJ(1b+2b+3b), SJ(1b+2b+3b+p), as well as BSJ(1b+2b) and BSJ(1b+2b+3b+p) trial wave functions. All energies are in Hartree per primitive unit cell.

gain of the various trial wave functions with respect to the SJ(1+2b) approach using the VMC and DMC methods for the two different systems are shown in Fig. 1. It is apparent that the addition of the three-body term and more so the p term substantially reduces the VMC energy, but that the DMC is only marginally affected since the initial nodal structure is identical. The usage of the BF transformation, however, improves the nodal surface and hence entails an energy lowering at the VMC and the DMC levels. Interestingly, the gain in energy for HS₂ is much more pronounced than for H₃S, which demonstrates the importance of an accurate trial wave function for the former. For the Im-3m phase of H₃S the energy gain is -1.634 and -0.56 eV at the VMC and DMC levels of theory, while for the C2/m HS₂ structure, the energy gain can be as high as -4.898 and -1.643 eV. The increased accuracy of the BF wave function, however, comes at a rather high computational cost, which is due to the necessity to evaluate the orbitals and their first two derivatives and moreover also the collective BF coordinates, because every element of the Slater matrix must be updated every time a single electron is moved. Even though it is partially compensated by the fact that the less complex BSJ(1b+2b) trial wave function is equally accurate than the much more complex SJ(1b+2b+3b+p) calculations,

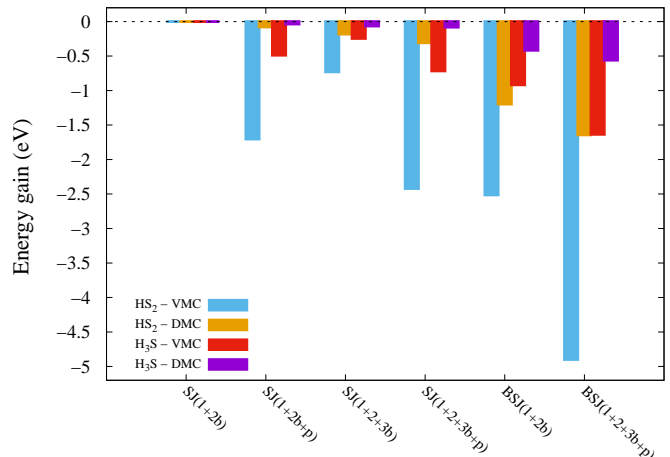


FIG. 1. (colour online) The reduction of variational energy for the HS₂ and H₃S systems using different trial wave functions with respect to the SJ(1b+2b) approach using the VMC and DMC methods.

we have elected to use the former instead of the latter in the following DMC calculations of the enthalpy-pressure phase diagram calculations.

C. DMC Enthalpy-Pressure Phase Diagram

In order to compute the enthalpy-pressure phase diagrams for the different structures, we fitted our extrapolated DMC total energies as a function of volume V against a model equations of state $E(V)$. We found that a quadratic polynomial is a sufficiently accurate representation of our actual DMC energies. Using this model, it is straightforward to calculate the pressure $P(V) = -dE(V)/dV$ as a function of V and thus also the enthalpy per atom $H = E + PV$.

In previous DFT calculations including ZPE correction it was predicted that at 200 GPa 5H₂S decomposes into 3H₃S and HS₂, where HS₂ adopts C2/c symmetry, but undergoes a phase transition to the more stable C2/m structure at 250 GPa²⁹. However, the present DMC enthalpies indicate that the C2/c HS₂ structure is more stable than the C2/m phase up to 440 GPa, as it is shown in Fig. 2. In fact, the enthalpy difference between the C2/c and C2/m phases of HS₂ is much larger than the ZPE correction as estimated by DFT²⁹.

Moreover, DFT-based crystal structure searches predict that the energetically most favorable phase of HS at 200 GPa is I4₁/amd and at 300 GPa C2/m²⁹. The present DMC enthalpy-pressure curves of HS are shown in Fig. 4. At variance to DFT, they suggest that the C2/m phase of HS is more stable than the I4₁/amd HS structure over the whole pressure range from 150 to 400 GPa. In fact, the difference in enthalpy between the C2/m and I4₁/amd phases is more than 600 meV/atom and is even larger with increasing pressure.

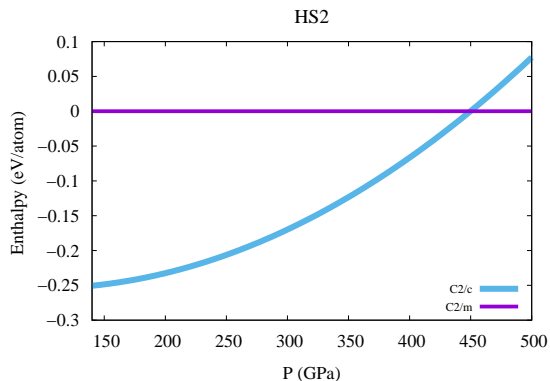


FIG. 2. (colour online) The DMC enthalpy as a function of pressure of the C2/c HS₂ structure relative to the C2/m phase. The estimated uncertainties in the DMC enthalpies due to statistical and systematic errors are represented by the widths of the corresponding lines.

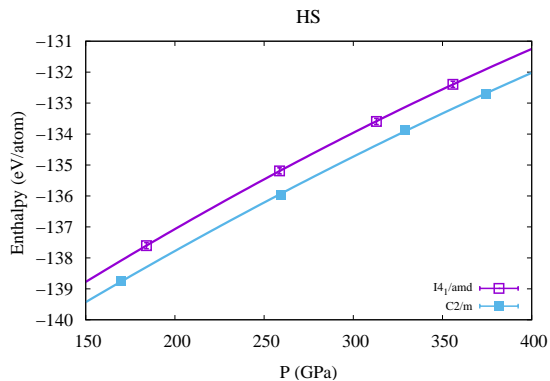


FIG. 3. (colour online) The DMC enthalpy of the C2/m and I₄/amd phases of HS as a function of pressure. The corresponding error bars are smaller than the size of the data points.

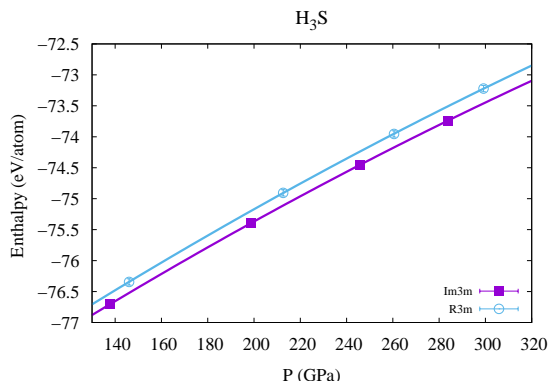


FIG. 4. (colour online) The DMC enthalpy of the Im-3m and R3m phases of H₃S as a function of pressure. The corresponding error bars are smaller than the size of the data points.

Previous crystal structure prediction calculations using DFT indicate that the R3m H₃S structure is stable at 130 GPa and that the Im-3m phase of H₃S is the most likely candidate at pressures larger than 200 GPa. Yet, our DMC enthalpy-pressure calculations again show that the Im-3m H₃S structure is the more favorable candidate up to at least 320 GPa, which is in agreement with very recent experimental results.²⁷

This is to say that altogether, our DMC results leads to a revision of the enthalpy-pressure phase diagram between 150 and 320 GPa. Specifically, we find that the C2/c HS₂, C2/m HS and Im-3m H₃S structures are energetically most favorable within the considered pressure range. However, it is well-known that the ZPE corrections plays an important role in the numerical determination of the phase diagram hydrogen-rich systems^{5,36,51}. Nevertheless, DFT calculations of others have shown that the energy difference between H₂S and S+H₂ due to ZPE is about 6 meV/f.u. at 160 GPa³¹, which is much smaller than our DMC enthalpy differences. We thus predict that the effect of ZPE on our DMC results is negligible.

IV. CONCLUSION

In summary, using highly accurate DMC calculations, we find that in the pressure range between 150 and 320 GPa, the C2/c HS₂, C2/m HS and the superconducting Im-3m H₃S structures are the enthalpically most favorable products of the decomposition of H₂S. Nevertheless, we conclude by noting that instead of the often proposed decomposition of H₂S into H₃S, HS₂, HS, or rather elemental S, the dissociation into H₃S⁺ and HS⁻ would be chemically much more sensible and still compatible with the recently performed XRD measurements²⁷.

ACKNOWLEDGMENTS

This work made use of computing facilities provided by ARCHER, the UK national super computing service, and by the High Performance Computing Service of Imperial College London, as well as of the OCuLUS system of the Paderborn Center for Parallel Computing (PC²). In particular, we acknowledge that the results of this research have been achieved using the PRACE-3IP project (FP7 RI-312763) resource ARCHER based in UK. Support from the Thomas Young Centre under grant number TYC-101 and EP/N50869X/1 is also thankfully acknowledged.

- * s.azadi@imperial.ac.uk
- ¹ J. Bardeen, L. N. Cooper and J. R. Schrieffer, *Phys. Rev.* **108**, 1175 (1957).
 - ² E. Wigner and H. B. Huntington, *J. Chem. Phys.* **3**, 764 (1935).
 - ³ N. W. Ashcroft, *Phys. Rev. Lett.* **21**, 1748 (1968).
 - ⁴ S. Azadi and T. D. Kühne, *JETP letters* **95**, 449 (2012).
 - ⁵ S. Azadi, W. M. C. Foulkes and T. D. Kühne, *New Journal of Physics* **15**, 113005 (2013).
 - ⁶ W. J. Nellis, S. T. Weir and A. C. Mitchell, *Science* **273**, 936 (1996).
 - ⁷ S. T. Weir, W. J. Nellis and A. C. Mitchell, *Phys. Rev. Lett.* **76**, 1860 (1996).
 - ⁸ W. J. Nellis, S. T. Weir and A. C. Mitchell, *Phys. Rev. B* **59**, 3434 (1999).
 - ⁹ M. I. Eremets and I. A. Troyan, *Nature Materials* **10**, 927 (2011).
 - ¹⁰ M. Zaghoo, A. Salamat and I. F. Silvera, *Phys. Rev. B* **93**, 155128 (2016).
 - ¹¹ N. W. Ashcroft, *Phys. Rev. Lett.* **92**, 187002 (2004).
 - ¹² J. Feng, W. Grochala, T. Jaron, R. Hoffmann, A. Bergara and N.W. Ashcroft, *Phys. Rev. Lett.* **96**, 017006 (2006).
 - ¹³ T. A. Strobel, P. Ganesh, M. Somayazulu, P. R. C. Kent and R. J. Hemley, *Phys. Rev. Lett.* **107**, 255503 (2011).
 - ¹⁴ R. T. Howie, P. Dalladay-Simpson and E. Gregoryanz, *Nature Materials* **14**, 495 (2015).
 - ¹⁵ C. Zha, Z. Liu and R. J. Hemley, *Phys. Rev. Lett.* **108**, 146402 (2012).
 - ¹⁶ M. I. Eremets, I. A. Trojan, S. A. Medvedev, J. S. Tse and Y. Yao, *Science* **319**, 1506 (2008).
 - ¹⁷ D. Y. Kim, R. H. Scheicher, C. J. Pickard, R. J. Needs and R. Ahuja, *Phys. Rev. Lett.* **107**, 117002 (2011).
 - ¹⁸ T. Scheler, O. Degtyareva, M. Marques, C. L. Guillaume, J. E. Proctor, S. Evans and E. Gregoryanz, *Phys. Rev. B* **83**, 214106 (2011).
 - ¹⁹ X. F. Zhou, A. R. Oganov, X. Dong, L. Zhang, Y. Tian and H. T. Wang, *Phys. Rev. B* **84**, 054543 (2011).
 - ²⁰ D. Y. Kim, R. H. Scheicher, H. k. Mao, T. W. Kang and R. Ahuja *Proc. Natl. Acad. Sci. U.S.A.* **107**, 2793 (2010).
 - ²¹ G. Gao, A. R. Oganov, P. Li, Z. Li, H. Wang, T. Cui, Y. Ma, A. Bergara, A. O. Lyakhov, T. Iitaka and G. Zou, *Proc. Natl. Acad. Sci. U.S.A.* **107**, 1317 (2010).
 - ²² G. Gao, A. R. Oganov, A. Bergara, M. Martinez-Canales, T. Cui, T. Iitaka, Y. Ma and G. Zou, *Phys. Rev. Lett.* **101**, 107002 (2008).
 - ²³ A. P. Drozdov, M. I. Eremets, I. A. Troyan, V. Ksenofontov and S. I. Shylin, *Nature* **525**, 73 (2015).
 - ²⁴ J. G. Bednorz and K. A. Mueller, *Z. Phys. B* **64**, 189 (1986).
 - ²⁵ A. Schilling, M. Cantoni, J. D. Guo and H. R. Ott, *Nature* **363**, 56 (1993).
 - ²⁶ L. Gao, Y. Y. Xue, F. Chen, Q. Xiong, R. L. Meng, D. Ramirez, C. W. Chu, J. H. Eggert and H. K. Mao, *Phys. Rev. B* **50**, 4260(R) (1994).
 - ²⁷ M. Einaga, M. Sakata, T. Ishikawa, K. Shimizu, M. I. Eremets, A. P. Drozdov, I. A. Troyan, N. Hirao and Y. Ohishi, *Nature Physics* **3760**, XXX (2016).
 - ²⁸ D. Duan, Y. Liu, F. Tian, D. Li, X. Huang, Z. Zhao, H. Yu, B. Liu, W. Tian and T. Cui, *Scientific Reports* **4**, 6968 (2014).
 - ²⁹ I. Errea, M. Calandra, C. J. Pickard, J. Nelson, R. J. Needs, Y. Li, H. Liu, Y. Zhang, Y. Ma and F. Mauri, *Phys. Rev. Lett.* **114**, 157004 (2015).
 - ³⁰ I. Errea, M. Calandra and F. Mauri, *Phys. Rev. Lett.* **111**, 177002 (2013).
 - ³¹ Y. Li, J. Hao, H. Liu, Y. Li and Y. Ma, *J. Chem. Phys.* **140**, 174712 (2014).
 - ³² C. J. Pickard and R. J. Needs, *Nature Physics* **3**, 473 (2007).
 - ³³ D. Duan, X. Huang, F. Tian, D. Li, H. Yu, Y. Liu, Y. Ma, B. Liu and T. Cui, *Phys. Rev. B* **91**, 180502(R) (2015).
 - ³⁴ X.-J. Chen, J.-L. Wang, V. V. Struzhkin, H.-k. Mao, R. J. Hemley and H.-Q. Lin, *Phys. Rev. Lett.* **101**, 077002 (2008).
 - ³⁵ M. Martinez-Canales, A. R. Oganov, Y. Ma, Y. Yan, A. O. Lyakhov and A. Bergara, *Phys. Rev. Lett.* **102**, 087005 (2009).
 - ³⁶ S. Azadi and W. M. C. Foulkes, *Phys. Rev. B* **88**, 014115 (2013).
 - ³⁷ M. A. Morales, J. M. McMahon, C. Pierleoni and D. M. Ceperley, *Phys. Rev. B* **87**, 184107 (2013).
 - ³⁸ R. C. Clay, J. Mcminis, J. M. McMahon, C. Pierleoni, D. M. Ceperley and M. A. Morales, *Phys. Rev. B* **89**, 184106 (2014).
 - ³⁹ S. Azadi, and R. E. Cohen, *J. Chem. Phys.* **145**, 064501 (2016).
 - ⁴⁰ D. M. Ceperley and B. J. Alder, *Phys. Rev. Lett.* **45**, 566 (1980).
 - ⁴¹ W. M. C. Foulkes, L. Mitas, R. J. Needs and G. Rajagopal, *Rev. Mod. Phys.* **73**, 33 (2001).
 - ⁴² M. Marchi, S. Azadi, M. Casula and S. Sorella, *J. Chem. Phys.* **131**, 154116 (2009).
 - ⁴³ M. D. Brown, J. R. Trail, P. López Ríos and R. J. Needs, *J. Chem. Phys.* **126**, 224110 (2007).
 - ⁴⁴ J. R. Trail and R. L. Needs, *J. Chem. Phys.* **128**, 204103 (2008).
 - ⁴⁵ S. Azadi, R. Singh and T. D. Kühne, *Int. J. Quantum Chem.* **115**, DOI: 10.1002/qua.25005 (2015).
 - ⁴⁶ S. Azadi and R. E. Cohen, *J. Chem. Phys.* **143**, 104301 (2015).
 - ⁴⁷ M. Marchi, S. Azadi and S. Sorella, *Phys. Rev. Lett.* **107**, 086807 (2011).
 - ⁴⁸ E. Mostaani, N. D. Drummond and V. I. Falkó, *Phys. Rev. Lett.* **115**, 115501 (2015).
 - ⁴⁹ S. Azadi and W. M. C. Foulkes, *J. Chem. Phys.* **143**, 102807 (2015).
 - ⁵⁰ N. D. Drummond, B. Monserrat, J. H. Lloyd-Williams, P. Lópes Ríos and R. J. Needs, *Nature Comm.* **6**, 7749 (2015).
 - ⁵¹ S. Azadi, B. Monserrat, W. M. C. Foulkes, and R. J. Needs, *Phys. Rev. Lett.* **112**, 165501 (2014).
 - ⁵² J. M. McMahon, M. A. Morales, C. Pierleoni and D. M. Ceperley, *Rev. Mod. Phys.* **84**, 1607 (2012).
 - ⁵³ S. J. Clark, M. D. Segall, C. J. Pickard, P. J. Hasnip, M. J. Probert, K. Refson and M. C. Payne, *Z. Kristallogr.* **220**, 567 (2005).
 - ⁵⁴ D. Vanderbilt, *Phys. Rev. B* **41**, 7892 (1990).
 - ⁵⁵ J. P. Perdew, K. Burke and M. Ernzerhof, *Phys. Rev. Lett.* **77**, 3865 (1996).
 - ⁵⁶ R. J. Needs, M. D. Towler, N. D. Drummond and P. López Ríos, *J. Phys.: Condens. Matter* **22**, 023201 (2010).

- ⁵⁷ J. R. Trail and R. J. Needs, *J. Chem. Phys.* **122**, 174109 (2005).
- ⁵⁸ J. R. Trail and R. J. Needs, *J. Chem. Phys.* **122**, 014112 (2005).
- ⁵⁹ S. Azadi, C. Cavazzoni and S. Sorella, *Phys. Rev. B* **82**, 125112 (2010).
- ⁶⁰ D. Alfè and M. J. Gillan, *Phys. Rev. B* **70** 161101, (2004).
- ⁶¹ N. D. Drummond, M. D. Towler and R. J. Needs, *Phys. Rev. B* **70**, 235119 (2004).
- ⁶² P. López Ríos, A. Ma, N. D. Drummond, M. D. Towler and R. J. Needs, *Phys. Rev. E* **74**, 066701 (2006).
- ⁶³ C. J. Umrigar, K. G. Wilson and J. W. Wilkins, *Phys. Rev. Lett.* **60**, 1719 (1988).
- ⁶⁴ N. D. Drummond and R. J. Needs, *Phys. Rev. B* **72**, 085124 (2005).
- ⁶⁵ C. Lin, F. H. Zong and D. M. Ceperley, *Phys. Rev. E* **64**, 016702 (2001).
- ⁶⁶ N. D. Drummond, R. J. Needs, A. Sorouri and W. M. C. Foulkes, *Phys. Rev. B* **78**, 125106 (2008).
- ⁶⁷ F. Calcavecchia, F. Pederiva, M. H. Kalos and T. D. Kühne, *Phys. Rev. E* **90**, 053304 (2014).
- ⁶⁸ F. Calcavecchia and T. D. Kühne, *Eur. Phys. Lett.* **110**, 20011 (2015).
- ⁶⁹ R. P. Feynman and M. Cohen, *Phys. Rev.* **102**, 1189 (1956).
- ⁷⁰ M. Holzmann, D. M. Ceperley, C. Pierleoni and K. Esler, *Phys. Rev. E* **68**, 046707 (2003).
- ⁷¹ M. Taddei, M. Ruggeri, S. Moroni and M. Holzmann, *Phys. Rev. B* **91**, 115106 (2015).